ORNL/TM-2015/97

Light Water Reactor Sustainability Program

Advanced Numerical Model for Irradiated Concrete

Alain B. Giorla

March 2015
U.S. Department of Energy
Office of Nuclear Energy

ORNL/TM-2015/97

Light Water Reactor Sustainability Program
Fusion and Materials for Nuclear Systems Division

ADVANCED NUMERICAL MODEL FOR IRRADIATED CONCRETE

Alain B. Giorla

March 2015

Prepared by
OAK RIDGE NATIONAL LABORATORY
P.O. Box 2008
Oak Ridge, Tennessee 37831-6285
managed by
UT-Battelle, LLC
for the
US DEPARTMENT OF ENERGY
Office of Nuclear Energy
under contract DE-AC05-00OR22725

Light Water Reactor Sustainability Program
Fusion and Materials for Nuclear Systems Division

ADVANCED NUMERICAL MODEL FOR IRRADIATED CONCRETE

ORNL/TM-2015/97
LWRS-M3LW-15OR0403044

March 2015

J.T. Busby — March 2015
Name — Date
Title [optional]

P. Ferguson — March 2015
Name — Date
Title [optional]

Name — Date
Title [optional]

Name — Date
Title [optional]

CONTENTS

LIST OF FIGURES

LIST OF TABLES

ACRONYMS

AMIE	Automated Mechanics Integrated Environment
ASR	Alkali-Silica Reaction
ITZ	Interfacial Transition Zone
NPP	Nuclear Power Plants
RIVE	Radiation-Induced Volumetric Expansion

EXECUTIVE SUMMARY

Several nuclear power plants in the United States are entering a phase of second renewal of their operating licenses. This would extent their service life from 60 to 80 years, which imposes long-term safety requirements on each and every component of the plants. Notably, a section of the concrete biological shield is directly exposed to the radiation from the reactor, which raises the question of the resistance of concrete again irradiation.

Several studies from the sixties and the seventies have shown that concrete exhibits a very high expansion when exposed to high levels of radiation (around one order of magnitude higher than more common durability phenomena in concrete), complemented in some cases with a loss of mechanical strength and stiffness. These effects, extensively documented by Field et al. [2015], typically occur at a high-energy neutron fluence around 10^{19}n/cm^2. A certain number of power plants are expected to reach such values after 80 years of operation. Understanding the effect of irradiation on concrete becomes therefore critical to assess the safety and operation of these plants.

The results of the aforementioned concrete irradiation experiments are not directly applicable to the analysis of nuclear power plant structures. These experiments were indeed carried out in very specific environmental conditions (temperature, relative humidity) and on a relatively short time scale compared to a structure service life, and in some cases with materials not necessarily representative of the concrete used in United States nuclear facilities. A careful analysis of these experiments is therefore required in order to understand the constitutive mechanisms of concrete swelling under irradiation, and then transpose it to the structural scale.

The expansion of concrete seemed mainly to be caused by the swelling of its aggregates. In a previous study, Le Pape et al. [2015] used mechanical homogenization schemes to correlate the swelling of the aggregates and of the corresponding concrete. This approach showed promising results, and offers a good first-order approximation for a very small computational cost. However, this method remains limited as it cannot predict simultaneously both the expansion and the damage in the material. Therefore, more elaborate tools are required to get a deeper understanding of the underlying mechanisms.

The macroscopic expansion and material properties (elasticity, strength, etc) of concrete can be obtained by numerical simulations at the level of the concrete mesoscale. In the present work, the material microstructure is represented with a finite element software AMIE (Automated Mechanics Integrated Environment) initially developed at the École Polytechnique Fédérale de Lausanne. With this framework, the aggregates are explicitly represented in the mesh as inclusions embedded in the cement paste, which allows to finely capture geometrical interactions between aggregates of different sizes as well as the localization of cracks and damage. The constitutive behavior of both phases (aggregates and cement paste) is independently characterized, and can be refined to account for the influence of various physical parameters (neutron fluence, temperature, humidity, strain rate, etc) on its properties. In this approach, the aggregates swelling is imposed as a function of the neutron fluence using experimental results from the literature, and the outputs of the simulation are the macroscopic expansion and loss of mechanical properties (elasticity, strength) of the concrete.

A specific attention is given to phenomena which compete one against another so that their respective influence is accurately estimated:

- **Damage vs. Relaxation:** the cement paste can relief stress either by visco-elastic stress relaxation or by the opening and propagation of micro-cracks. The rate of deformation dictates which of the two mechanisms dominate.

- **Temperature vs. Relative Humidity:** the stress relaxation phenomenon in the cement paste is accelerated by high temperature, but slowed down by low relative humidity, which are the environmental conditions in which the irradiation experiments typically take place. Their balance might further affect the aforementioned damage-relaxation coupling.
- **Brittle vs. Ductile Failure:** the failure mechanism of concrete depends on the applied load rate, and might in some cases control the stability of the crack propagation in concrete.

These three points are critical for the extrapolation of the experimental results to actual structures, as both the environmental conditions (temperature, relative humidity) and loading rate differ.

In this report, we establish a numerical model for concrete exposed to irradiation to address these three critical points. The model accounts for creep in the cement paste and its coupling with damage, temperature and relative humidity. The shift in failure mode with the loading rate is also properly represented. The numerical model for creep has been validated and calibrated against different experiments in the literature [Wittmann, 1970, Le Roy, 1995]. Results from a simplified model are shown to showcase the ability of numerical homogenization to simulate irradiation effects in concrete.

In future works, the complete model will be applied to the analysis of the irradiation experiments of Elleuch et al. [1972] and Kelly et al. [1969]. This requires a careful examination of the experimental environmental conditions as in both cases certain critical information are missing, including the relative humidity history. A sensitivity analysis will be conducted to provide lower and upper bounds of the concrete expansion under irradiation, and check if the scatter in the simulated results matches the one found in experiments. The numerical and experimental results will be compared in terms of expansion and loss of mechanical stiffness and strength. Both effects should be captured accordingly by the model to validate it.

Once the model has been validated on these two experiments, it can be applied to simulate concrete from nuclear power plants. To do so, the materials used in these concrete must be as well characterized as possible. The main parameters required are the mechanical properties of each constituent in the concrete (aggregates, cement paste), namely the elastic modulus, the creep properties, the tensile and compressive strength, the thermal expansion coefficient, and the drying shrinkage. These can be either measured experimentally, estimated from the initial composition in the case of cement paste, or back-calculated from mechanical tests on concrete. If some are unknown, a sensitivity analysis must be carried out to provide lower and upper bounds of the material behaviour.

Finally, the model can be used as a basis to formulate a macroscopic material model for concrete subject to irradiation, which later can be used in structural analyses to estimate the structural impact of irradiation on nuclear power plants.

1. Introduction

The long-term operation of nuclear power-plants (NPP) requires to understand the various degradation phenomena that can affect such structures, and the ability to simulate these phenomena with accurate and predictive models. Several studies have shown that concrete exposed to radiation undergoes very large expansion as well as a loss of mechanical properties (elastic modulus, tensile and compressive strength), see [Field et al., 2015] for a comprehensive review. These effects are mostly caused by the expansion of the aggregates [Hilsdorf et al., 1978], and vary a lot from one aggregate type to another [Seeberger and Hilsdorf, 1982].

However, these experiments were conducted in specific conditions which may not be representative of the material as exposed in NPP. Among the parameters which may play a significant role are the temperature, the relative humidity, and possibly the irradiation rate. The evolution of these parameters differs widely from one experiment to another, and occur on a much shorter time scale as in structures. Because of the complexity of the material and its behavior (which is notably non linear and time-dependent), the extrapolation of the experimental data to real structures is not immediate.

In a recent paper, Le Pape et al. [2015] derived an analytic model for the expansion and loss of mechanical properties of irradiated concrete, using homogenization approaches based on the work of Mori and Tanaka [1973], Budiansky and O'Connell [1976]. These methods are limited in the sense that they consider the *average* values of the strain and stress fields, while the heterogeneous nature of the material and the high differential strains between the aggregates and the cement paste may lead to *local* stresses values much higher than the strength of the cement paste, and therefore micro-cracking. Additionally, the cement paste is a visco-elastic material and may be able to relieve part of these stresses through reversible processes. Characterizing the competition between damage and stress relaxation requires more advanced numerical tools and a representation of the mesostructure of the material.

Finite elements at the mesoscale have been used to study several concrete degradation phenomena, including strength [Du and Sun, 2007, Dupray et al., 2009, Nguyen et al., 2012], creep [Tran et al., 2013, Lavergne et al., in press], shrinkage [de Sa et al., 2008, Idiart et al., 2012, de Larrard et al., 2013, Maruyama and Sugie, 2014], leaching [Bernard et al., 2008], thermal damage [Grondin et al., 2011] or alkali-silica reaction (ASR) [Dunant and Scrivener, 2010, Wu et al., 2014, Giorla et al., 2015]. At this scale, concrete is represented by aggregates embedded into a cement paste matrix, sometimes with an additional interface transition zone (ITZ) using for example cohesive elements to simulate debonding of the aggregates. In this framework, the mechanical behaviors of each phase are kept as simple as possible; the complexity of the overall behavior derives from the micromechanical interactions between the different constituents, as well as possible gradient effects throughout the sample.

Salomoni et al. [2014] proposed a three-dimensional mesoscale model of irradiated-affected concrete using a coupled thermo-hygro-radiation model chained with a visco-damage mechanical model. Their simulation show strong gradients effects within irradiated samples, as the damage is mostly concentrated in a layer below the face exposed to the radiation. The thermo-hygro-radiation model proposed seems very robust and is able to characterize variations of temperature or radiation between the aggregates, the cement paste, and the ITZ. However, their model did not account for the aggregate radiation-induced volumetric expansion (RIVE), which for some aggregates can reach up to 1% for high neutron fluence. For comparison, the expansion found in ASR are around 0.1%, and is able to cause a significant amount of damage in the concrete microstructure. It seems therefore that the RIVEshould be included in numerical simulations of irradiated concrete, in order to capture both the expansion of the material and the internal damage.

In the present report, we show the basis for a more elaborate mesoscale model for concrete affected by

irradiation. A special attention is given to effects which may drastically affect the results of the simulation.

1.1 Modeling strategy

Numerical modeling of concrete at the mesoscale can be divided into four different main components, which can be independently investigated, modified, or refined depending on the goals of the simulations:

- **Mechanisms:** This is a set of constitutive equations which describe the physics of the system. It is constituted by a set of partial differential equations (which govern the evolution of the different unknown of the systems) complemented by a set of relations (which describe how the parameters of the partial differential equation evolve as a function of other physical parameters such as time, temperature, or neutron fluence). These relations can derive from fundamental principles (for example linear elasticity), or from empiric observations. This is the main focus of the current work.
- **Microstructure:** This refers to the sample geometry as well as the morphological and geometrical characteristics of the aggregates: particle size distribution, shape, position. In the present report, aggregates are represented with homogeneous circles, which is a limitation as most aggregates in the field are multi-phasic. However, accounting for aggregate heterogeneity requires additional information which are unknown at the present state of knowledge, such as the specific radiation-induced expansion of each mineral phase.
- **Conditions:** This includes the temperature, humidity, and radiation histories to which the sample is subject. They can be chosen to reflect experiments or actual structures. Note that in most cases, the evolution of the humidity is poorly known, and must be assumed. The present work does not aim to provide a complete coupling between thermo-hygro-radiation conditions and the mechanical fields. The temperature, humidity and radiation fields are taken as input of the model. They can be known from experiments, assumed, or approximated from results from other models.
- **Resolution:** This describes the numerical method used to solve the system of partial differential equations which describes the mechanisms. In the present work, we use finite elements, but alternative methods like fast Fourier transform [Moulinec and Suquet, 1994] or lattice elements [Schlangen and Garboczi, 1997] are possible.

1.2 Software implementation

The model is implemented in AMIE (Automated Mechanics Integrated Environment), an open-source C++ extended finite element library initially developed at the Ecole Polytechnique Fédérale de Lausanne. AMIE was developed for the mesoscale analysis of ASR in concrete [Dunant and Scrivener, 2010]. Its architecture was designed as a toolbox to test different mechanical behavior and extended finite elements [1] formulations, and is generic enough to be extensible to other phenomena like irradiation.

AMIE was designed with two goals in mind: i) generation of random concrete microstructures ii) resolution of partial differential equations with the finite element method. As a toolbox, it had a steep learning curve and required a strong background in C++ programming to use its full capabilities.

[1] Extended finite elements are used to simulate strong discontinuities in the mechanical fields such as cracks [Moës et al., 1999] or inclusions [Sukumar et al., 2001]. In the present work, the extended finite elements capabilities of AMIE are not required. They remain available for future works if needed, for example for coupled irradiation-ASR simulations.

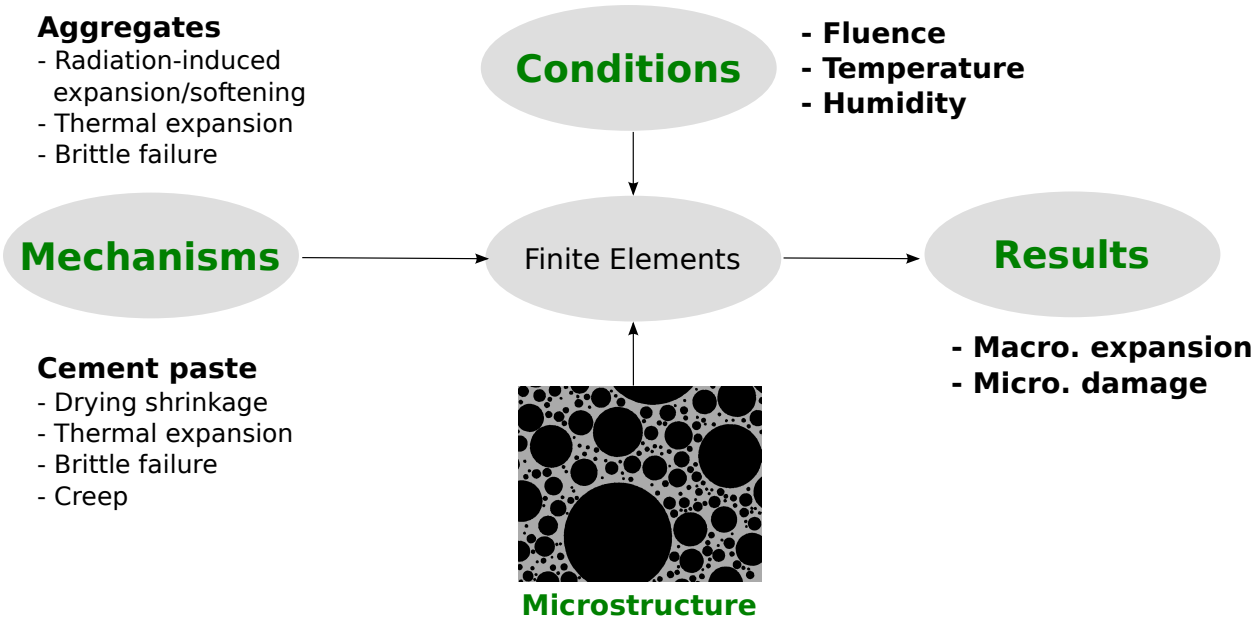

Figure 1. Numerical modeling strategy for irradiated concrete

Furthermore, it lacked the ability to use generic relations to describe the evolution of the material parameters (elasticity, strength, etc) with physical variables (without tinkering the code itself).

Therefore, in 2015, AMIE was extended to provide a framework for concrete mesoscale simulations that i) does not require programming from the end-user (unless said user needs very specific information) ii) is able to account for any generic relation between the mechanical parameters and the physical variables. While the list of mechanical parameters is limited (the set of constitutive partial differential equations is likely not subject to change), the physical variables and relations can be arbitrarily extended or reduced following the user's decision. Current physical variables are the temperature, relative humidity, and neutron fluence, but fields such as gamma radiation, capillary pressure, degree of hydration or concentration of certain species could be introduced if required.

Furthermore, a scripting language was written in order to control the simulation inputs, exchange these between researchers, or run the same simulations with a different values for some of the parameters.

This implementation effort was conducted in order to reduce the long-term development time, increase the research efficiency, and allow researchers without prior C++ knowledge to use AMIE.

1.3 Numerical resolution

AMIE uses finite elements in space and time to simulate time-dependent phenomena. Space-time finite elements were developed simultaneously [Argyris and Scharpf, 1969, Fried et al., 1969] with more conventional finite difference methods [Zienkiewicz et al., 1968, Bažant and Wu, 1974]. The later became more popular as their formulation requires less memory, which was the limiting factor in high-performance computing at the time. A few authors have applied space-time finite elements in the framework of solid mechanics, notably for the analysis of wave propagation [Hughes and Hulbert, 1988, French, 1993], frictional contact [Adélaïde et al., 2003], or generalized Maxwell materials [Idesman et al., 2001].

Using space-time finite elements has two advantages over standard finite difference schemes: i) it can reproduce with a greater accuracy geometries that change in time ii) the resulting problem scales easily with

the time step, which facilitates the calculation of time-step adaptative methods, as opposed to a finite difference scheme in which the system matrix must be re-assembled at each change of the time step.

The mathematical foundations for the space-time finite element method as implemented in AMIE can be found in [Giorla et al., 2014]. The formulation proposed uses continuous displacement in time, but discontinuous velocities. Using the Discontinuous Galerkin method[2] (in which both the displacements and velocities are continuous in time) would lead to more accurate results [Hughes and Hulbert, 1988], but at a much higher numerical cost, as the use of the jump operator in space and time would make the final system matrix asymmetric, as in [Idesman et al., 2001], and therefore forbid the use of efficient solvers. The current implementation leads to symmetric positive-definite system matrices. The system is then solved with the efficient conjugate gradient method [Hestenes and Stiefel, 1952]. This allows to approach large numerical problems (up to 10^6 degrees of freedom) on a standard workstation.

[2] a more generic numerical method to solve coupled space-time partial differential equations.

2. Mechanisms

In this section, we describe the mechanisms and relations which govern the behavior of each constituent of irradiated concrete. A special attention is given to mechanisms which compete one against each other, and which are summarized below:

- **Damage vs. Relaxation:** the cement paste has two mechanisms to relief high stresses: micro-cracking (damage) and visco-elastic dissipation (stress relaxation). These two have different consequences on the microstructure and the overall behavior, as the first is an irreversible process, while the second is (to some extent) reversible. The main consequence of stress relaxation is to reduce damage compared to a material which is not visco-elastic. This effect has already been shown for drying shrinkage [Benboudjema et al., 2005] and ASR [Giorla et al., 2015].

- **Temperature vs. Relative Humidity:** the visco-elastic properties of the material depend on both parameters. A higher temperature accelerates creep [Bengougam, 2002], while a lower relative humidity reduces the extent of the visco-elastic deformation [Wittmann, 1970]. During radiation experiments, the samples are under very high temperature but have been pre-dried (very low relative humidity). Therefore, the net effect on creep and stress relaxation must be properly captured.

- **Brittle vs Ductile Failure:** cement paste is typically modeled as a brittle material. However, tensile tests at different strain rates show that the material becomes more ductile for slower strain rates [Bazant and Gettu, 1992]. In simulations, brittle or ductile failure may have dramatic impact over the result, as the crack propagation may be unstable in the first case, stable in the second [Giorla et al., 2015]. Therefore, the ductility of the material as function of the strain rate must be properly accounted for.

Following are the set of partial differential equations and relations which govern the material behavior. Fourth-order tensors are described with double-barred capital letters (e.g. $\mathbb{C}, \mathbb{E}$), second-order tensors with bold greek letters (e.g. $\boldsymbol{\sigma}$, $\boldsymbol{\epsilon}$), scalars as italic roman letters or normal-font greek letters (e.g. d, T, ϵ).

2.1 Cement paste

We consider only mature, fully hydrated cement pastes as the focus of this study is the long-term behavior of the material. Effect of hydration on the material properties are therefore not accounted for in the model.

The strain $\boldsymbol{\epsilon}$ in the cement paste is decomposed into five independent components:

$$\boldsymbol{\epsilon} = \boldsymbol{\epsilon}_e + \boldsymbol{\epsilon}_v + \boldsymbol{\epsilon}_r + (\epsilon_T + \epsilon_h)\,\mathbf{1} \tag{1}$$

Where $\boldsymbol{\epsilon}_e$ is the elastic strain, $\boldsymbol{\epsilon}_v$ the non recoverable (viscous) creep strain, $\boldsymbol{\epsilon}_r$ the recoverable creep strain, ϵ_T the thermal expansion, ϵ_h the drying shrinkage, and $\mathbf{1}$ the unit second-order tensor. The decomposition in different mechanisms is shown in Figure 2.

First, we show the set of constitutive partial differential equations which govern the problem (sections 2.1.1 to 2.1.3). Then, we show how the different material properties are influenced by the physical variables (sections 2.1.4 to 2.1.8).

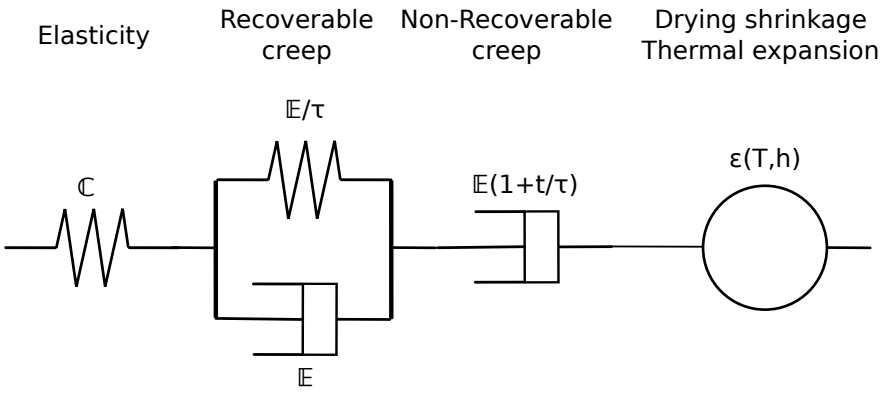

Figure 2. Rheological model for the cement paste

2.1.1 Elastic deformation

The relation between the elastic strain and the stress $\boldsymbol{\sigma}$ is straightforward:

$$\boldsymbol{\sigma} = \mathbb{C}_e : \boldsymbol{\epsilon}_e \tag{2}$$

Where $\mathbb{C}_e$ is the fourth-order stiffness tensor of the material.

2.1.2 Creep deformation

The creep deformation is divided into two different components:

- a viscous flow $\boldsymbol{\epsilon}_v$, which causes a long-term non recoverable deformation,
- a visco-elastic deformation $\boldsymbol{\epsilon}_r$ which can be recovered if the material is unloaded.

The overall creep curve of cement paste follows a logarithmic curve in time, see for example [Le Roy, 1995, Vandamme and Ulm, 2009]. The presence of the non recoverable deformation implies that the creep of the material does not follow exactly the Boltzmann superposition principle, as what is typically seen in practice for concrete [Neville, 1971, Bažant and Wittmann, 1982].

From a modeling perspective, the long-term deformation can be represented by an hardening dashpot [Bazant and Baweja, 2000]:

$$\boldsymbol{\sigma} = (1 + \gamma)\, \mathbb{E}_v : \dot{\boldsymbol{\epsilon}}_v \tag{3}$$

Where γ is the hardening variable, and $\mathbb{E}_v$ the initial fourth-order viscosity tensor of the material. The rate of hardening is assumed constant, which after integration, gives rise to a creep logarithmic in time:

$$\dot{\gamma} = \frac{1}{\tau_v} \tag{4}$$

Where τ_v is the characteristic time of the long-term creep deformation.

The recoverable part of the deformation is approximated with a single Kelvin-Voigt unit. Other models consider more elaborate formulations (e.g. [Bazant and Baweja, 2000]), but the distinction between

recoverable and irrecoverable creep deformations is not always possible in practice. The constitutive equation of this Kelvin-Voigt module is:

$$\boldsymbol{\sigma} = \mathbb{C}_r : [\boldsymbol{\epsilon}_r + \tau_r \, \dot{\boldsymbol{\epsilon}}_r] \tag{5}$$

Where $\mathbb{C}_r$ is the fourth-order stiffness tensor of the spring in the Kelvin-Voigt unit, and τ_r the characteristic time of the dashpot. This approach was notably used by Hilaire et al. [2014], who also adjusted the value of $\mathbb{C}_r$ as a function of the hydration degree. As the focus of the present study is mature cement paste, the dependency to the hydration degree is neglected.

These two properties can be measured experimentally from creep curves containing an unloading section. However, this is generally not available, so the following approximation is used in the model, and still provides a good approximation of the creep curve of the material:

$$\tau_r = \tau_v \tag{6}$$

$$\mathbb{C}_r = \frac{1}{\tau_r}\mathbb{E}_v \tag{7}$$

2.1.3 Continuum damage

We consider cement paste as a pseudo-brittle material with a linear softening branch. We consider an isotropic scalar damage variable d, as at this scale, possible anisotropy is induced by geometrical effects rather than anisotropy of the behaviors themselves. The damage variable affects equally all mechanical properties[3]:

$$\mathbb{C}_e(d) = (1-d)\,\mathbb{C}_e^0 \tag{8}$$

$$\mathbb{C}_r(d) = (1-d)\,\mathbb{C}_r^0 \tag{9}$$

$$\mathbb{E}_v(d) = (1-d)\,\mathbb{E}_v^0 \tag{10}$$

Where the index ^{0} denotes the undamaged material properties.

The linear softening branch is governed by two independent variables: the strength at the peak f^t, and the ultimate strain ϵ_y^t at the end of the branch. The index ^{t} denotes the properties in tension, while ^{c} indicates failure in compression.

Damage increases when the stress-strain history of the material reaches the linear softening surface. This can be expressed with the following criteria:

$$C^t = \|\boldsymbol{\sigma}\|^t - \frac{f^t}{f^t - \mathrm{E}^0\epsilon_y^t}\mathrm{E}^0\left(\|\boldsymbol{\epsilon}\|^t - \epsilon_y^t\right) \tag{11}$$

$$C^c = \|\boldsymbol{\sigma}\|^c - \frac{f^c}{f^c - \mathrm{E}^0\epsilon_y^c}\mathrm{E}^0\left(\|\boldsymbol{\epsilon}\|^c - \epsilon_y^c\right) \tag{12}$$

Where C^t and C^c are the failure criteria in tension and compression of the material, E^0 the undamaged Young's modulus of the material (related to its elastic stiffness tensor $\mathbb{C}_e$), $\|.\|^t$ and $\|.\|^c$ are the maximum and minimum principal averaged stresses or strains.

[3]This corresponds to the hypothesis that cement paste itself is an homogeneous material [Tsien, 1950]. A different repartition of damage between elastic and viscoelastic properties might be found if the heterogeneity of the paste were to be considered

The propagation conditions read:

$$\dot{d} \geq 0 \tag{13}$$
$$C^t \leq 0 \tag{14}$$
$$C^c \leq 0 \tag{15}$$
$$\dot{d} \times \max\left(C^t,\, C^c\right) = 0 \tag{16}$$

In practice, only the strength of the material can be measured, and, in some cases, the total fracture energy G^t. The later is related to the strength and the ultimate strain by the area under the softening curve:

$$G^t = \frac{1}{2} f^t \left[\epsilon_y^t - \frac{f^t}{\mathrm{E}^0}\right] \tag{17}$$

The model is made non local by using averaged values for the stresses and strains in (11-12). Non local damage models [Pijaudier-Cabot and Bažant, 1987] are used to avoid mesh-sensitiveness and spread the damage in the simulation over a certain damage process zone, which is a material characteristic. The averaging procedure is the following, as suggested by Jirásek [1998]:

1. The total strain field $\boldsymbol{\epsilon}$ is averaged over a certain distance r using a truncated polynomial [Peerlings et al., 2001], giving $\bar{\boldsymbol{\epsilon}}$.
2. The averaged stress field $\bar{\boldsymbol{\sigma}}$ is obtained from the averaged strain field $\bar{\boldsymbol{\epsilon}}$ and the *local* values of the visco-elastic, thermal and drying strains and the *local* mechanical properties. The local values must be used, otherwise gradients in shrinkage or expansion may not induced damage.
3. The principal components of the averaged strain and stress fields are then extracted.

The averaging distance r is a material parameter which has an important influence over the final damage pattern.

2.1.4 Effect of temperature

Thermal expansion causes the material to expand by ϵ_T, obtained by the following relation:

$$\epsilon_T = \alpha_T \left(T - T_0\right) \tag{18}$$

Where α_T is the linear thermal expansion coefficient and T_0 the reference temperature at which the material properties were measured.

Note that at high temperature (above 200°C), the material suffers an apparent contraction instead of an expansion. This is not caused by a change in α_T but by the additional shrinkage induced by the evaporation of water in the material microstructure. The coefficient α_T itself seems mostly unaffected by the temperature [Harmathy and Berndt, 1966].

Elastic modulus Harmathy and Berndt [1966] showed that the modulus of elasticity of the cement pastes with various compositions did not change significantly up to 200°C, temperature above which the modulus of elasticity drops significantly, notably induced by micro-cracking around portlandite grains [Piasta, 1984]. However, this change is mostly caused by the evaporation of water from the microstructure, and is therefore addressed in section 2.1.5 which covers the influence of relative humidity.

Creep Various studies have shown that creep is accelerated under high temperature, e.g. [Maréchal, 1969, Bengougam, 2002]. From a numerical perspective, the effect of temperature on creep can be simulated with an Arrhenius-type law:

$$\tau_v(T) = \exp\left(T_a\left(\frac{1}{T} - \frac{1}{T_0}\right)\right)\tau_v(T_0) \tag{19}$$

Where T_a is an "activation temperature" for creep. The same relation is applied to τ_r.

Bazant and Baweja [2000] suggests a value of 5,000K, but this value is likely to change from one cement to another. For comparison, Bengougam [2002] measured activation temperatures of 6,000 and 17,000K for concrete cores extracted from hydraulic power plants. Given the wide range of activation temperatures found, and the fact that this parameter is generally unknown for the materials considered, its influence must be carefully estimated.

Strength Komonen and Penttala [2003] measured the compressive and flexural strength of cement paste at elevated temperature. They found that the strength first decreases, reaches a minimum around 100°C, after which it increases again and plateaus between 200 and 400°C, then finally decreases exponentially towards 0.

In compression, the first minimum is around 75% of the initial strength, and the plateau is approximately equal to that initial value. In flexion, the loss of strength is more dramatic, as the first minimum is around 25% of the initial strength, and the plateau around 50%.

As these effects are likely to be caused by variations in the water content of the sample, they are not directly accounted in the model, but result from the in the relative humidity (see section 2.1.5).

2.1.5 Effect of relative humidity

Reduction of relative humidity h causes the material to shrink by ϵ_h, obtained by the following relation:

$$\epsilon_h = \alpha_h\left(\min_t(h(t)) - h_0\right),\ h < h_0 \tag{20}$$

Where α_h is the strain when the material is completely dried, and h_0 is the reference humidity. We assume that the shrinkage is entirely irreversible, which is only true when the material is exposed to high drying conditions (see for example [Naus, 2010]).

A number of authors prefer to consider drying shrinkage as a function of the mass water content in the material rather than the relative humidity [Torrenti et al., 1997, Maruyama, 2010] or the capillary pressure [Benboudjema et al., 2005, Coussy et al., 2004, Gawin et al., 2007]. However, both these models require to know the sorption-desorption isotherms of the material, which varies with temperature [Poyet, 2009] and shows a strong hysteresis [Baroghel-Bouny et al., 1997].

Elastic modulus The stiffness of the material depends strongly on its water content. Maruyama et al. [2014a,b] found that the evolution of the mechanical properties of dried cement paste followed three stages as the relative humidity decreases: the modulus first increases, then decreases (up to reaching its initial, saturated, value), and finally increases as the microstructure collapses and densifies. However, Beaudoin et al. [2010] found that the modulus of dried cement paste decreases monotonously with the relative humidity of the material.

Furthermore, it is likely that the rate of drying has a certain impact on the apparent modulus of the dried paste. Indeed, micro-cracks can be observed around the portlandite grains in heat-dried pastes [Piasta, 1984], which would cause a decrease in elastic properties. Maruyama et al. [2014a,b] used a slower drying method

(9 month cure at constant relative humidity) than Beaudoin et al. [2010] (oven-dried at 110°C), which might reduce this micro-cracking through stress relaxation effects.

In absence of further evidence, the effect of relative humidity on the elastic properties are ignored in a first approximation.

Creep The creep of the cement paste is reduced with a lower water content in the sample [Wittmann, 1970, Tamtsia and Beaudoin, 2000]. From the analysis of Wittmann's experiments, we use the following formula to model the influence of relative humidity on the creep properties of the material:

$$\mathbb{E}_v(h) = \left[\frac{1-h}{h_1} + \exp\left(\frac{h-1}{h_1}\right)\right]\mathbb{E}_v(1) \tag{21}$$

Where h_1 is a constant with the same dimensions of a relative humidity, and controls the amount of creep at 0% relative humidity. The same relation is applied to $\mathbb{C}_r$.

The present model indicates that the material still exhibits creep deformations at 0% relative humidity, as found by Wittmann. This is debatable, as Acker and Ulm [2001], Tamtsia and Beaudoin [2000] suggest the opposite. The dried cement pastes in Tamtsia and Beaudoin experiments still show some creep deformation, albeit with a much smaller amplitude than what Wittmann measured. Therefore, the model might be subject to change if further experimental evidence is gathered.

Note that this effect is different from the Pickett effect [1942], which is the increase of the creep deformation of *concrete* in drying condition. This increase is caused by micro-cracking induced by gradients in relative humidity across the samples as well as the restraining effect of the aggregates [Skoczylas et al., 2007]. As a mesoscale effect, it is expected to be an output of the model, rather than an input. Therefore, the drying creep is not accounted for in the constitutive behavior of the cement paste.

Strength As the other mechanical properties of cement paste, strength is strongly affected by the water content. However, most studies focus on the mechanical behavior of dried concrete or mortar, in which additional effects such as micro-cracking occur. Maruyama et al. [2014a,b] measured the compressive and flexural strength of slowly dried cement paste, and found that it followed a similar evolution than the elastic modulus. Drying at high temperature leads to a curve with a similar shape but with a lower amplitude [Komonen and Penttala, 2003]. This could be an effect of micro-cracking caused by the thermal shock. In absence of further evidence and appropriate model in the literature, this effect is neglected in a first approximation.

Thermal expansion The content of water in the material affects the apparent coefficient of thermal expansion, as the thermal expansion of water can be partially accommodated by changes in saturation and capillary pressure. The coefficient of thermal expansion is maximum for intermediate values of the relative humidity, and decreases when the humidity either increases or decreases. Grasley and Lange [2007] analyzed this effect using poro-mechanics, and found the following relation between the coefficient of thermal expansion α_T and the relative humidity h:

$$\alpha_T(h) = \alpha_T(1) - h\,\ln(h)\frac{\mathrm{R}}{\mathrm{m}_w}\left(\frac{1}{3\,k} - \frac{1}{k_s}\right) \tag{22}$$

Where R is the universal gas constant, m_w the molar volume of liquid water (in a first approximation not function of the temperature), k the bulk modulus of the cement paste (obtained from the elastic tensor $\mathbb{C}_e$), and k_s the bulk modulus of the solid skeleton of the cement paste.

2.1.6 Effect of strain rate

The loading rate has an impact on the fracture characteristic of concrete [Bazant and Gettu, 1992, Denarié et al., 2006]. At higher strain rate, the strength is higher, but the material becomes more fragile. The crack pattern is also modified, as fast loading rates produce diffuse micro-cracks while slow lading rate lead to the opening of a single localized crack. For very slow loading rates, the material apparently behaves as a pseudo-plastic material, with very limited stress softening. This shift of behavior can have a critical impact on the simulated results, as the softening curve of the material defines the stability of the crack propagation, as found by the author in the context of ASR [Giorla et al., 2015].

In order to simulate this effect, the strength of the material and the ultimate strains are defined as function of the current strain rate in the material:

$$f^t = f_0^t \left(0.6 + 0.4 \left|\frac{\dot{\epsilon}}{\dot{\epsilon}_0}\right|^p\right) \tag{23}$$

$$\epsilon_y^t = \frac{f_{y,0}^t}{\mathrm{E}} \left(1 + \log_{10}\left(\left|\frac{\dot{\epsilon}_0}{\dot{\epsilon}}\right|\right)\right) \tag{24}$$

Where p is an exponent between 0 and 1 which controls the decrease of strength with the strain rate, and ϵ_0 is the reference strain rate at which the properties were measured. Similar expressions are used for the failure in compression.

With this model, the cement paste is considered as purely brittle for fast strain rates, and becomes progressively more ductile as the strain rate decreases. The material ultimately tends towards a pseudo-plastic behavior for infinitely slow loading rates.

2.1.7 Effect of neutron radiation

Both Kelly et al. [1969] and Elleuch et al. [1972] measured a shrinkage of the cement paste as well as a reduction of the elastic modulus under radiation. However, it was determined that this loss of mechanical properties was identical in samples subject to the same thermal history, without radiation. Therefore, we assume that the neutron radiation has no effect on the cement paste.

However, Pedersen [1971] observed the disappearance of portlandite cluster in irradiated specimen, which might have some impact on the overall mechanical properties of the paste. This, however, could be an artifact of Pedersen experiments caused by the conditions of temperature and humidity in the irradiation rig.

2.1.8 Effect of gamma radiation

The primary effect of gamma radiation is the radiolysis of the water contained in the material, even when the paste has been pre-dried [Elleuch et al., 1972]. The rate of gas emission generally decreases in time under irradiation. Kontani et al. [2013] found it dependent on the the gamma dose rate as well as the water content in the sample.

Lowinska-Kluge and Piszora [2008] showed that the cement hydrates deteriorate under gamma irradiation, including crystalline phases such as portlandite and tobermorite. The degree of damage was found to be increasing for higher dose rates. Vodák et al. [2005, 2011] also reported a loss of crystallinity and a refinement of the porosity, which was attributed to 'radiation-induced carbonation'. However, Bouniol et al. [2013] showed that this carbonation effect does not occur at temperature above 45°C, and therefore would not happen in NPP.

A few authors have tried to characterize the effects of gamma radiation on the mechanical properties, see e.g. [Gray, 1971, Kelly et al., 1969, Vodák et al., 2005]. Observations range from no noticeable effects to small losses of strength. However, in most cases the environmental conditions of the material are poorly known or controlled, and the loss of mechanical properties could be attributed to pure drying and carbonation rather than gamma-induced effects.

A noticeable experiment is the autogenous shrinkage and creep experiment under gamma radiation of McDowall [1971]. The samples were in mixed sealing condition, with the use of a bubbler which was used to prevent moisture loss while allowing gas evaporation. In this setup, the autogenous shrinkage of the irradiated sample was higher, but the creep was also lowered. This is contradictory with the Pickett effect which states that the rate of drying creep is higher for faster drying rates [Day et al., 1984].

There seems to be a strong gap of knowledge on the exact effects of gamma radiation on cement paste, notably because of the difficulty to decorelate radiation effects from natural drying and carbonation. Therefore, there will be no attempt in the present work to simulate these effects.

2.2 Aggregates

The mechanical behavior of the aggregates is simply described as an elastic-brittle material. The strain is simply decomposed as:

$$\boldsymbol{\epsilon} = \boldsymbol{\epsilon}_e + (\epsilon_T + \epsilon_\mathrm{n})\,\mathbf{1} \tag{25}$$

Where ϵ_n is the radiation-induced volumetric expansion (RIVE).

The material follows linear elasticity (section 2.1.1) and linear softening continuum damage mechanics (section 2.1.3) as described above. The creep of the aggregates are ignored in a first approximation as most aggregates do not show time-dependent deformations. The rheological model for the aggregates is shown in Figure 3.

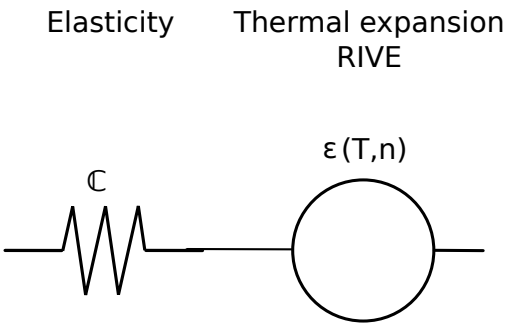

Figure 3. Rheological model for the aggregates

Most aggregates remain stable by the temperature in the ranges considered [Naus, 2010], therefore the mechanical properties of the aggregates are not affected by the temperature in the model. Potential drying shrinkage is also neglected, even though this approximation is not valid for the most porous aggregates [Maruyama and Sugie, 2014]. Also, gamma radiation is likely to have no effect on the aggregates as well because of their low content of water. Finally, most rocks do not exhibit a time-dependent behavior (at least in static conditions) [Bažant et al., 1993]. Therefore, only the effect of neutron fluence is to be determined.

2.2.1 Effect of neutron radiation

The morphology of the mineral phases contained in the aggregates is profoundly modified by the radiation. Disorders occur so that crystalline phases become amorphous. This reduced the mechanical properties of the aggregates (notably Young's modulus and tensile and compressive strength), but also induces a very high volumetric swelling, see for example [Elleuch et al., 1972, Hilsdorf et al., 1978, Kelly et al., 1969]. The magnitude of the effects depends on the mineralogy of the aggregates, as some phases seem to be more sensitive to radiation than the others [Gray, 1971, Seeberger and Hilsdorf, 1982]. In some cases, the failure behavior of the mineral seem to change, and might even present a hardening phase before rupture [Seeberger and Hilsdorf, 1982].

The RIVEis assumed to follow an S-shape curve as proposed by Zubov and Ivanov [1966] for quartz:

$$\epsilon_{\mathrm{n}} = \frac{\kappa_{\mathrm{n}}\ \epsilon_{\mathrm{n,max}} \left(e^{\delta_{\mathrm{n}} \cdot \mathrm{n}} - 1 \right)}{\epsilon_{\mathrm{n,max}} + \kappa_{\mathrm{n}}\ e^{\delta_{\mathrm{n}} \cdot \mathrm{n}}} \tag{26}$$

Where $\epsilon_{\mathrm{n,max}}$ controls the final expansion, κ_{n} controls the slope of the curve, and δ_{n} is a scale parameter.

Concerning the loss of mechanical properties, there is no model available in the current state of knowledge, and the exact effects vary a lot from one aggregate to another. Therefore, these are accounted for in the model using experimental data when available.

The radiation-induced amorphisation also greatly enhances the dissolution of the mineral phases, which might promote ASR [Ichikawa and Koizumi, 2002]. This effect will be ignored in a first step of the model, but is a potential future development of the model.

2.2.2 Effect of aggregate morphology

In the present model, the aggregates are considered as circles with homogeneous isotropic mechanical properties. However, most aggregates are polyphasic, and in some cases, they may present a strong anisotropy, either in shape or in properties.

Anisotropy is typically induced by a foliated microstructure (it is the case, for example, of the serpentine aggregates used by Elleuch et al. [1972] in their radiation experiments). This not only causes the material to be weaker in the direction perpendicular to the foliation, it may also produce aggregates with elongated shapes and sharp angles during the crushing process [Guimaraes et al., 2007]. This in turn affects the apparent failure behavior of the simulated concrete, as Du and Sun [2007] showed that the material was more brittle with sharp elongated aggregates rather than with circles due to stress concentration effects.

The simulation of multiphasic aggregates might induce internal differential stresses in the aggregates (as it is for example the case in ASR) followed by micro-cracking. This would have a profound influence in the morphology and kinetics of the overall damage. In the current state of knowledge, the expansion of different minerals in the aggregates are poorly known, and the mineral composition of the aggregates is generally not available for the experiments in the literature. This effect is therefore ignored in a first approximation until further data become available.

2.3 Summary

Table 1 references all possible effects and interactions on the various phenomena represented in the model. Color indicates whether a specific effect is accounted for (green), accounted for with an empyrical law (blue), not accounted for (black), not accounted for with potential strong influence on the results (red) and unknown (orange).

Phase	Parameter	Elasticity	Creep	Fracture	Imposed deformations
Paste	Temperature	strong	strong	strong	strong
	Relative humidity	strong	strong	strong	strong
	Strain rate	none	none	strong	small
	Neutron radiation	small	unknown	small	small
	Gamma radiation	small	medium	small	small
Aggregates	Temperature	small	generally none	small	small
	Relative humidity	small	generally none	medium	small
	Strain rate	generally none	generally none	small	none
	Neutron radiation	strong	generally none	strong	strong
	Gamma radiation	small	generally none	small	small
	Morphology	small	generally none	strong	medium

Table 1. Interactions between environmental conditions and physical phenomena for the cement paste and the aggregates.

The main missing components are:

- Influence of high temperature and relative humidity on the elastic and strength properties of cement paste: this varies from one cement to another, and might also be subject to strong rate effects. Simulating these effects might require a certain number of parameters which are not easily known or commonly measured, such as the sorption-desorption isotherm of the hardened cement paste. Also, the cement used in the irradiation experiment of Elleuch et al. [1972] is a very specific aluminate cement which exact properties with respect to temperature or relative humidity are poorly described.
- Influence of radiation on the cement paste creep: the only known experiment is the creep test under gamma radiation of McDowall [1971], in which drying and creep occur simultaneously. This experiment requires an appropriate analysis to separate both effects.
- Aggregate morphology: multiphasic aggregates might have a strong influence on the final crack pattern. However, there is no sufficient data at this point to simulate the aggregate microstructure properly.

3. Model calibration and validation

The different components of the model were validated and calibrated on different experiments of the literature.

3.1 Creep model

We use the experimental results of the extensive study of Le Roy [1995] to validate the creep model developed above. Le Roy measured the basic creep of a large set of concretes, varying the cement paste composition, aggregate content, or water/cement ratio, as well as the creep of the corresponding cement pastes.

We use the experimental creep curves for cement paste to calibrate our model, and then perform a numerical creep test on a concrete microstructure with the same cement properties, and compare the creep of the simulated concrete with the corresponding experimental value.

The composition of the three concretes is shown in Table 2, where w/c is the water-to-cement ratio, SF the amount of silica fume added to the mix (as a mass fraction of cement), and f_g the aggregate volumetric fraction. The samples were loaded at 28 days and sealed, so we ignore hydration effects as well as shrinkage in a first approximation.

Cement paste The material properties for the cement paste are obtained from the basic creep curves measured for the corresponding paste. We assume the Poisson ratio of all tensors in the material model ν_e, ν_r, ν_v to be equal to 0.2 as an arbitrary value since only uni-axial creep curves produced in this work. This leaves only three parameters which are easily read on the experimental curves: E_e the elastic Young's modulus (read from the initial deformation), η_v the uni-axial viscosity (read from the slope of the asymptotic creep curve), and τ_v the characteristic time of the viscous processes (read as the instant at which the initial and final asymptotes intersect).

Mix	w/c	SF	f_g	E_e [GPa]	E_v [GPa]	τ_v [d]
B0	0.5	0	0.705	12	30	3.3
B6	0.28	0.1	0.71	25	70	4.1
B7	0.38	0.1	0.713	17	80	2.5

Table 2. Composition of the concrete mixes and material parameters for the corresponding cement pastes from Le Roy [1995].

Aggregates The aggregates are simulated as purely elastic materials with a Young's modulus of 77 GPa as measured by Le Roy, and a Poisson ratio of 0.2 in absence of further data.

Sample and microstructure generation The samples used in the concrete creep experiments were cylinders 16 cm in diameter and 100 cm in length. Since we cannot simulate both the entire sample and the entire aggregate particle size distribution, we limit ourselves to a 8×8 cm square slices of the same sample, in which the entire particle size distribution of the material is represented. The ITZ is neglected, and the aggregates and the paste are assumed to be perfectly bonded. The left edge of the simulated sample

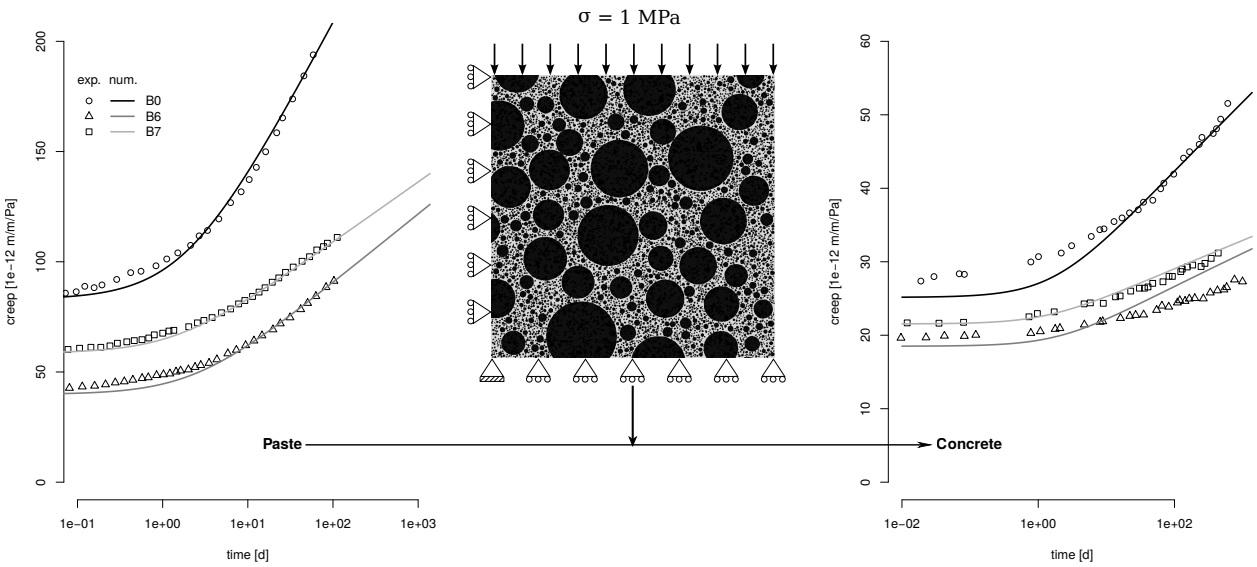

Figure 4. Experimental and numerical creep curves for cement paste (left) and concrete (right). Experimental data from [Le Roy, 1995]. The microstructure for the concrete B0 and the boundary conditions applied to the numerical concrete sample are shown in the middle.

corresponds to the vertical axis of the cylinder, so its horizontal displacement is set to 0. The aggregate particle size distribution in the simulation follows the distribution measured given by Le Roy, and the volume fraction of aggregates is the same in the simulations and in the experiments. The boundary conditions and simulated microstructure for the B0 concrete are shown in Figure 4.

Results Figure 4 shows on the left the experimental creep curve for the cement paste and the model calibrated using the values found in Table 2, and the experimental and numerical creep curves at the concrete level on the right. We obtain a good agreement between the experimental and simulated creep, except for the concrete B6 for which the model predict a higher creep. However, this could be related to additional shrinkage, since this specific material has a very low water/cement ratio, and therefore a very high autogeneous shrinkage as noticed by Le Roy in his work. Furthermore, the creep before the logarithmic trend is in general underestimated, but this could be related to the choice of characteristic time for the recoverable creep.

3.2 Influence of relative humidity on creep

The effect of relative humidity on the creep of the cement paste is validated on the set of experiments by Wittmann [1970], in which he studied the creep of sealed cement paste specimens pre-dried at a relative humidity ranging from 0 to 0.985. We fitted each creep curve separately using the same characteristic time (found equal to 2 days). Wittmann did not measure the elastic properties of its material, therefore only the viscous modulus η_v can be extracted from his experiments. The evolution of the $\eta_v(h)/\eta_v(h = 0.985)$ against the relative humidity is shown in Figure 5.

From this curve, we identified the relation between the creep properties and the humidity proposed in section 2.1.5. The comparison between the model and the experimental creep data is shown in Figure 6, with

the material properties in Table 3. We obtain a good agreement between the simulated values and the experiments for all levels of relative humidity.

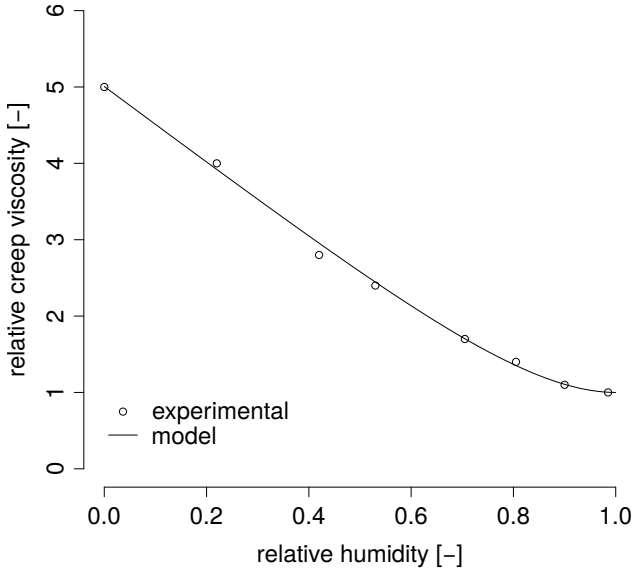

Figure 5. Effect of relative humidity on creep modulus of cement paste. Experimental data from Wittmann [1970].

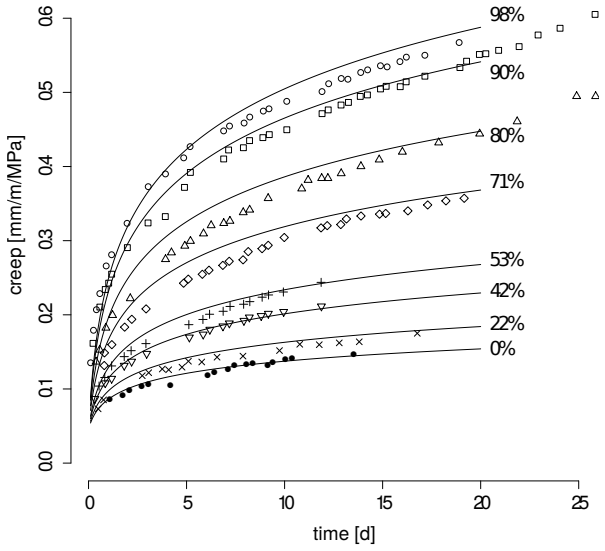

Figure 6. Effect of relative humidity on the creep of pre-dried cement pastes. Experimental data from Wittmann [1970].

Property		Value [Unit]
Viscous uni-axial viscosity	η_v	35 [GPa.d]
Viscous characteristic time	τ_v	2 [d]
Relative humidity creep coefficient	h_0	0.2 [-]

Table 3. Model parameters for the effect of relative humidity on creep calibrated on the experiments of Wittmann [1970].

3.3 Further requirements

The following effects require further calibration and validation:

- Strain recovery: the creep model presented above shows a partial strain recovery when a sample is unloaded, which corresponds qualitatively to what is observed in real concrete. Simulation of strain recovery experiments are still required to prove that the model captures quantitatively this effect.
- Rate-dependent fracture: the creep-damage coupling model presented above shows the same features as what was observed experimentally by Bazant and Gettu [1992], Denarié et al. [2006]. Simulations are still required to validate this effect and calibrate the parameter of the model.

4. Preliminary results

The following numerical examples showcase the ability of the model to simulate the effect of irradiation at the mesoscale. We use the experiments of Elleuch et al. [1972] as an example of the model. In these simulations, we do not used the entire model; rather, we start with the most simple model (purely elastic) and increase progressively the number of phenomena the model accounts for.

4.1 Materials

Cement paste: In these experiments, the cement used is not a traditional Portland cement, but an aluminate cement which was chosen for its ability to withstand high temperatures. Elleuch et al. provided several material properties for the cement paste, including pulse velocity (which can be correlated to a Young's modulus), compressive and tensile strength, and thermal expansion coefficient. The drying shrinkage and creep of the material are unknown, and therefore are calibrated to a value similar to what was measured for high-performance cement pastes by Le Roy [1995].

Aggregates: Elleuch et al. used a serpentine aggregates and measured their physical properties (modulus, strength, thermal exapsnion coefficient) before and after irradiation. We use these results as an input in the model in order to properly characterize the loss of stiffness as a function of the irradiation. The aggregate is slightly anisotropic with respect to its foliation, but this effect is ignored here.

Concrete We simulate in a first approximation a square sample containing 40% of aggregates. This is not representative of the actual experiment (66%), but this fraction and the coarse mesh (around 3,000 elements) permit fast simulations so that the model can be easily tested.

4.2 Conditions

We reproduce as close as possible the environmental conditions in which these experiments were carried out. Five phases can be distinguished:

1. 3 month cure at 0.6 relative humidity and 20°C
2. Pre-drying at 250°Cwith a slow heating rate (relative humidity unknown)
3. Preparation for the irradiation experiments (temperature, relative humidity and duration unknown)
4. Irradiation set by three short steps in temperature and neutron fluence (relative humidity unknwon)
5. Cooling phase (rate and duration unknown)

In their experiments, Elleuch et al. measured the expansion and loss of material properties between phase 3 and 5. In the simulation, we also measure the expansion between these two instants so that the experimental and numerical results can be directly compared.

Figure 7 shows the evolution of the temperature, neutron fluence and relative humidity as a function of time. The relative humidity history is assumed to be a succession of logarithmic curves based upon the temperature history.

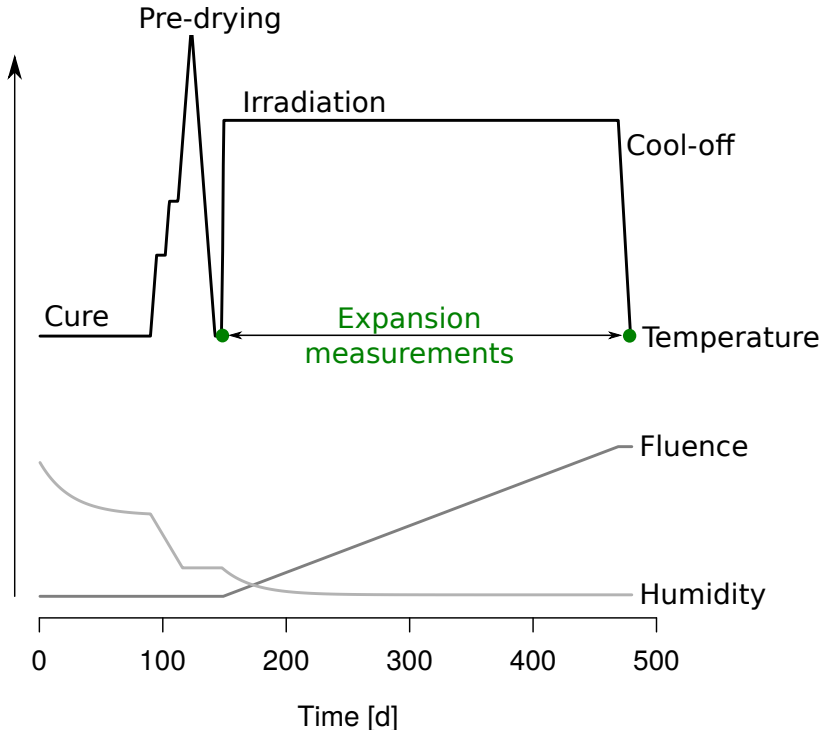

Figure 7. Environmental conditions in the experiments of Elleuch et al. [1972]. Relative humidity history is assumed.

4.3 Results

We use three simplified models in a first approximation:

1. Purely elastic: the creep and damage properties of all phases are ignored.
2. Purely visco-elastic: the damage properties of all phases are ignored. The influence of temperature and relative humidity on creep are accounted for.
3. Purely elastic-brittle: the creep properties of all phases are ignored. All materials are assumed to be perfectly brittle (as opposed to the linear softening branch proposed above) and the influence of strain rate on the fracture properties are ignored.

The expansion as a function of the fluence is shown for the three cases in Figure 8. We show that even with these simple models, the trend is properly captured. The simulated results show a lower expansion than in the experiments, but that may be caused by the low fraction of aggregates in the sample, as well as the incomplete state of the model. Indeed, both creep and damage tend to increase the simulated expansion. These effects would be further enhanced with an appropriate creep-damage coupling.

Figure 9 shows the damage pattern resulting from the purely elastic-brittle simulation. The pattern shows heavy cracking between the aggregates, which suggests that the material is entirely broken at the end of the irradiation. However, these simulations are an higher bound of the damage. The brittle behavior as well as the very coarse mesh makes the sample much more fragile that it would be with a more advanced model.

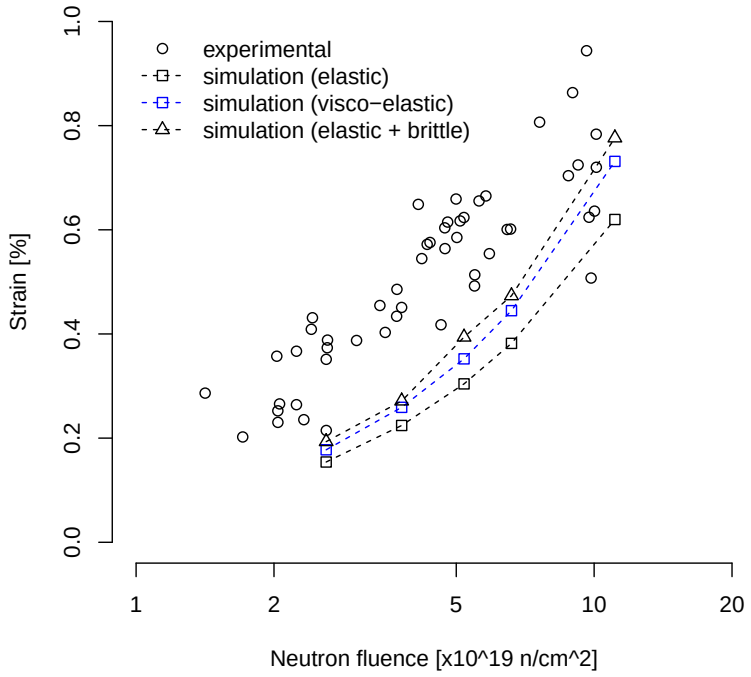

Figure 8. Numerical and experimental radiation-expansion curves. Experimental data from [Elleuch et al., 1972].

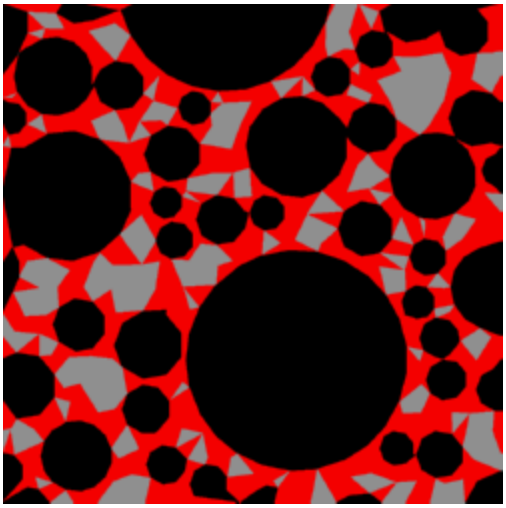

Figure 9. Damage pattern obtained with the elastic-brittle model. Black: aggregates. Grey: sound cement paste. Red: Damaged cement paste.

5. Conclusion and perspectives

In this report, we develop a numerical model for the mesoscale simulation of concrete irradiation. A comprehensive description of the model was given to serve as a basis for future simulations and developments. The model distinguishes between cement paste and aggregates, and uses a finite element representation of the concrete mesostructure. The model accounts for the influence of temperature and humidity on the creep of the cement paste, and of neutron irradiation on the swelling and mechanical properties of the aggregates. The output of the model is the concrete expansion and loss of mechanical properties as a function of the environmental conditions (neutron fluence, temperature, humidity).

The model for the creep of the cement paste was validated on experiments from the literature, but more calibration is still required, notably on the influence of strain rate on the material strength. We highlighted that in most irradiation experiments from the literature, a certain number of material properties and data are missing, including the creep and drying shrinkage of the cement paste, as well as the relative humidity history the samples are subject to. This requires a careful examination of the influence of each parameters on the overall simulation by the use of lower and upper bounds values.

Finally, we showed that a simplified model can still partially capture the expansion caused by irradiation. This illustrates the ability of the model to simulate irradiation effects in concrete as well as the need for a more refined and robust model.

The model can be used to analyze experiments of concrete irradiation such as the experiments of Kelly et al. [1969] or Elleuch et al. [1972]. This work is done in collaboration with Michaela Vaitova, a civil engineering PhD. candidate at the Czech Technical University of Prague under the supervision of Petr Stemberk. The analysis of these experiments will be the subject of a publication in Nuclear Engineering and Design, which is currently being drafted.

After validation and calibration on these experiments, the model can then be applied to simulate the environmental conditions representative of NPP. This would require beforehand a proper characterization of the material properties of the concrete considered and its constituents, or a sensitivity analysis for properties than cannot be measured. The model can also be used as a basis to formulate a macroscopic concrete model, which in turn could be used for structural analysis of NPP.

References

P. Acker and F.-J. Ulm. Creep and shrinkage of concrete: physical origins and practical measurements. *Nuclear Engineering and Design*, 203(2):143–158, 2001.

L. Adélaïde, F. Jourdan, and C. Bohatier. Frictional contact solver and mesh adaptation in space–time finite element method. *European Journal of Mechanics-A/Solids*, 22(4):633–647, 2003.

J. Argyris and D. Scharpf. Finite elements in time and space. *Nuclear Engineering and Design*, 10(4): 456–464, 1969.

V. Baroghel-Bouny, B. Perrin, and L. Chemloul. Détermination expérimentale des propriétés hydriques des pates de ciment durcies—mise en evidence des phénomenes d'hystérésis. *Materials and Structures*, 30 (200):340–348, 1997.

Z. Bazant and S. Baweja. Creep and shrinkage prediction model for analysis and design of concrete structures: Model B3. *ACI SPECIAL PUBLICATIONS*, 194:1–84, 2000.

Z. Bazant and R. Gettu. Rate effects and load relaxation in static fracture of concrete. *ACI Materials Journal*, 89(5):456–468, 1992.

Z. Bažant and F. Wittmann. *Creep and shrinkage in concrete structures*. Wiley Chichester, 1982.

Z. Bažant and S. Wu. Rate-type creep law of aging concrete based on maxwell chain. *Matériaux et Construction*, 7(1):45–60, 1974.

Z. Bažant, B. Shang-Ping, and R. Gettu. Fracture of rock: effect of loading rate. *Engineering Fracture Mechanics*, 45(3):393–398, 1993.

J. Beaudoin, L. Raki, R. Alizadeh, and L. Mitchell. Dimensional change and elastic behavior of layered silicates and portland cement paste. *Cement and Concrete Composites*, 32(1):25–33, 2010.

F. Benboudjema, F. Meftah, and J. Torrenti. Interaction between drying, shrinkage, creep and cracking phenomena in concrete. *Engineering structures*, 27(2):239–250, 2005.

A. Bengougam. *Déformations différées et effets d'échelle des bétons de barrage*. PhD thesis, Ecole Polytechnique Fédérale de Lausanne, n°2624, 2002.

F. Bernard, S. Kamali-Bernard, and W. Prince. 3d multi-scale modelling of mechanical behaviour of sound and leached mortar. *Cement and Concrete Research*, 38(4):449–458, 2008.

P. Bouniol, B. Muzeau, and V. Dauvois. Experimental evidence of the influence of iron on pore water radiolysis in cement-based materials. *Journal of Nuclear Materials*, 437(1):208–215, 2013.

B. Budiansky and R. O'Connell. Elastic moduli of a cracked solid. *International Journal of Solids and Structures*, 12(2):81–97, 1976.

O. Coussy, P. Dangla, T. Lassabatère, and V. Baroghel-Bouny. The equivalent pore pressure and the swelling and shrinkage of cement-based materials. *Materials and Structures*, 37(1):15–20, 2004.

R. Day, P. Cuffaro, and J. Illston. The effect of rate of drying on the drying creep of hardened cement paste. *Cement and Concrete Research*, 14(3):329–338, 1984.

T. de Larrard, B. Bary, E. Adam, and F. Kloss. Influence of aggregate shapes on drying and carbonation phenomena in 3d concrete numerical samples. *Computational Materials Science*, 72:1–14, 2013.

C. de Sa, F. Benboudjema, M. Thiery, and J. Sicard. Analysis of microcracking induced by differential drying shrinkage. *Cement and Concrete Composites*, 30(10):947–956, 2008.

E. Denarié, C. Cécot, and C. Huet. Characterization of creep and crack growth interactions in the fracture behavior of concrete. *Cement and concrete research*, 36(3):571–575, 2006.

C. Du and L. Sun. Numerical simulation of aggregate shapes of two-dimensional concrete and its application 1. *Journal of Aerospace Engineering*, 20(3):172–178, 2007.

C. Dunant and K. Scrivener. Micro-mechanical modelling of alkali–silica-reaction-induced degradation using the amie framework. *Cement and Concrete Research*, 40(4):517–525, 2010.

F. Dupray, Y. Malecot, L. Daudeville, and E. Buzaud. A mesoscopic model for the behaviour of concrete under high confinement. *International journal for numerical and analytical methods in geomechanics*, 33 (11):1407–1423, 2009.

L. Elleuch, F. Dubois, and J. Rappeneau. Effects of neutron radiation on special concretes and their components. *Special Publication of The American Concrete Institute*, 43:1071–1108, 1972.

K. Field, I. Remec, and Y. Le Pape. Radiation Effects on Concrete for Nuclear Power Plants, Part I: Quantification of Radiation Exposure and Radiation Effects. *Nuclear Engineering and Design*, 282: 126–143, 2015.

D. French. A space-time finite element method for the wave equation. *Computer methods in applied mechanics and engineering*, 107(1):145–157, 1993.

I. Fried, M. Cremer, and P. McMurtry. Finite-element analysis of time-dependent phenomena. *AIAA Journal*, 7(6):1170–1173, 1969.

D. Gawin, F. Pesavento, and B. Schrefler. Modelling creep and shrinkage of concrete by means of effective stresses. *Materials and Structures*, 40(6):579–591, 2007.

A. Giorla, K. Scrivener, and C. Dunant. Finite elements in space and time for the analysis of generalised visco-elastic materials. *International Journal for Numerical Methods in Engineering*, 97(6):454–472, 2014.

A. Giorla, K. Scrivener, and C. Dunant. Influence of visco-elasticity on the stress development induced by alkali–silica reaction. *Cement and Concrete Research*, 70:1–8, 2015.

Z. Grasley and D. Lange. Thermal dilation and internal relative humidity of hardened cement paste. *Materials and Structures*, 40(3):311–317, 2007.

B. Gray. The effects of reactor radiation on cements and concrete. In *Inf. Exchange Meeting on Results of Concrete Irradiation Programmes*, pages 17–39. Commission of the European Communities, 1971.

F. Grondin, H. Dumontet, A. Ben Hamida, and H. Boussa. Micromechanical contributions to the behaviour of cement-based materials: Two-scale modelling of cement paste and concrete in tension at high temperatures. *Cement and Concrete Composites*, 33(3):424–435, 2011.

M. Guimaraes, J. Valdes, A. Palomino, and J. Santamarina. Aggregate production: fines generation during rock crushing. *International journal of mineral processing*, 81(4):237–247, 2007.

T. Harmathy and J. Berndt. Hydrated portland cement and lightweight concrete at elevated temperatures. *Journal of the American Concrete Institute*, 63(1):93–112, 1966.

M. Hestenes and E. Stiefel. Methods of conjugate gradients for solving linear systems. *Journal of Research of the National Bureau of Standards*, 49(6):409–436, 1952.

A. Hilaire, F. Benboudjema, A. Darquennes, Y. Berthaud, and G. Nahas. Modeling basic creep in concrete at early-age under compressive and tensile loading. *Nuclear Engineering and Design*, 269:222–230, 2014.

H. Hilsdorf, J. Kropp, and H. Koch. The effects of nuclear radiation on the mechanical properties of concrete. *Special Publication of The American Concrete Institute*, 55:223–254, 1978.

T. Hughes and G. Hulbert. Space-time finite element methods for elastodynamics: formulations and error estimates. *Computer methods in applied mechanics and engineering*, 66(3):339–363, 1988.

T. Ichikawa and H. Koizumi. Possibility of radiation-induced degradation of concrete by alkali-silica reaction of aggregates. *Journal of Nuclear Science and Technology*, 39(8):880–884, 2002.

A. Idesman, R. Niekamp, and E. Stein. Finite elements in space and time for generalized viscoelastic maxwell model. *Computational Mechanics*, 27(1):49–60, 2001.

A. Idiart, J. Bisschop, A. Caballero, and P. Lura. A numerical and experimental study of aggregate-induced shrinkage cracking in cementitious composites. *Cement and Concrete Research*, 42(2):272–281, 2012.

M. Jirásek. Nonlocal models for damage and fracture: comparison of approaches. *International Journal of Solids and Structures*, 35(31):4133–4145, 1998.

B. Kelly, J. Brocklehurst, D. Mottershead, S. McNearney, and I. Davidson. The effects of reactor radiation on concrete. In *Proceedings of the Second Information Meeting on Pre Stress Concrete and Reactor Pressure Vessels and their Thermal Isolation, Brussels*, pages 237–265, 1969.

J. Komonen and V. Penttala. Effects of high temperature on the pore structure and strength of plain and polypropylene fiber reinforced cement pastes. *Fire technology*, 39(1):23–34, 2003.

O. Kontani, S. Sawada, I. Maruyama, M. Takizawa, and O. Sato. Evaluation of irradiation effects on concrete structure: Gamma-ray irradiation tests on cement paste. In *ASME 2013 Power Conference*. American Society of Mechanical Engineers, 2013.

F. Lavergne, K. Sab, J. Sanahuja, M. Bornet, and C. Toulemonde. Inverstigation of the effect of aggregates' morphology on concrete creep properties by numerical simulations. *Cement and Concrete Research*, in press.

Y. Le Pape, K. Field, and I. Remec. Radiation Effects in Concrete for Nuclear Power Plants - Part II: Perspective from Micromechanical Modeling. *Nuclear Engineering and Design*, 282:144–157, 2015.

R. Le Roy. *Déformations instantanées et différées des bétons à hautes performances*. PhD thesis, École Nationale des Ponts et Chaussées, 1995.

A. Lowinska-Kluge and P. Piszora. Effect of gamma irradiation on cement composites observed with xrd and sem methods in the range of radiation dose 0-1409 mgy. *Acta Physica Polonica-Series A General Physics*, 114(2):399, 2008.

J. Maréchal. Le fluage du béton en fonction de la température. *Matériaux et Construction*, 2(2):111–115, 1969.

I. Maruyama. Origin of drying shrinkage of hardened cement paste: hydration pressure. *Journal of Advanced Concrete Technology*, 8(2):187–200, 2010.

I. Maruyama and A. Sugie. Numerical study on drying shrinkage of concrete affected by aggregate size. *Journal of Advanced Concrete Technology*, 12(8):279–288, 2014.

I. Maruyama, Y. Nishioka, G. Igarashi, and K. Matsui. Microstructural and bulk property changes in hardened cement paste during the first drying process. *Cement and Concrete Research*, 58:20–34, 2014a.

I. Maruyama, H. Sasano, Y. Nishioka, and G. Igarashi. Strength and young's modulus change in concrete due to long-term drying and heating up to 90 ^{o}C. *Cement and Concrete Research*, 66:48–63, 2014b.

D. McDowall. The effect of gamma irradiation on the creep properties of concrete. In *Inf. Exchange Meeting on Results of Concrete Irradiation Programmes*, pages 55–69. Commission of the European Communities, 1971.

N. Moës, J. Dolbow, and T. Belytschko. A finite element method for crack growth without remeshing. *Int. J. Numer. Meth. Engng*, 46:131–150, 1999.

T. Mori and K. Tanaka. Average stress in matrix and average elastic energy of materials with misfitting inclusions. *Acta metallurgica*, 21(5):571–574, 1973.

H. Moulinec and P. Suquet. A fast numerical method for computing the linear and nonlinear mechanical properties of composites. *Comptes rendus de l'Académie des sciences. Série II, Mécanique, physique, chimie, astronomie*, 318(11):1417–1423, 1994.

D. Naus. *A Compilation of Elevated Temperature Concrete Material Property Data and Information for Use in Assessments of Nuclear Power Plant Reinforced Concrete Structures*. US Nuclear Regulatory Commission, Office of Nuclear Regulatory Research, 2010.

A. Neville. *Creep of concrete: plain, reinforced, and prestressed*. North Holland Publishing, Amsterdam, 1971.

V. Nguyen, M. Stroeven, and L. Sluys. Multiscale failure modeling of concrete: micromechanical modeling, discontinuous homogenization and parallel computations. *Computer Methods in Applied Mechanics and Engineering*, 201:139–156, 2012.

A. Pedersen. Radiation damage in concrete: Measurements on miniature specimens of cement mortar. In *Inf. Exchange Meeting on Results of Concrete Irradiation Programmes*, pages 5–16. Commission of the European Communities, 1971.

R. Peerlings, M. Geers, R. De Borst, and W. Brekelmans. A critical comparison of nonlocal and gradient-enhanced softening continua. *International Journal of Solids and Structures*, 38(44):7723–7746, 2001.

J. Piasta. Heat deformations of cement paste phases and the microstructure of cement paste. *Matériaux et Construction*, 17(6):415–420, 1984.

G. Pickett. The effect of change in moisture-content on the creep of concrete under a sustained load. In *ACI Journal Proceedings*, volume 38. ACI, 1942.

G. Pijaudier-Cabot and Z. Bažant. Nonlocal damage theory. *Journal of Engineering Mechanics*, 113(10): 1512–1533, 1987.

S. Poyet. Experimental investigation of the effect of temperature on the first desorption isotherm of concrete. *Cement and Concrete Research*, 39(11):1052–1059, 2009.

V. Salomoni, C. Majorana, B. Pomaro, G. Xotta, and F. Gramegna. Macroscale and mesoscale analysis of concrete as a multiphase material for biological shields against nuclear radiation. *International Journal for Numerical and Analytical Methods in Geomechanics*, 38(5):518–535, 2014.

E. Schlangen and E. Garboczi. Fracture simulations of concrete using lattice models: computational aspects. *Engineering fracture mechanics*, 57(2):319–332, 1997.

J. Seeberger and H. Hilsdorf. Einfluss von radioaktiver strahlung auf die festigkeit und struktur von beton. Technical Report NR2505, Institüt fur Massiubau und Baustofftechnologie, Arbeitlung Boustofftechnologie, Universität Karlsruhe, Germany, 1982.

F. Skoczylas, N. Burlion, and I. Yurtdas. About drying effects and poro-mechanical behaviour of mortars. *Cement and Concrete Composites*, 29(5):383–390, 2007.

N. Sukumar, D. Chopp, N. Moës, and T. Belytschko. Modeling holes and inclusions by level sets in the extended finite-element method. *Computer methods in applied mechanics and engineering*, 190(46): 6183–6200, 2001.

B. Tamtsia and J. Beaudoin. Basic creep of hardened cement paste a re-examination of the role of water. *Cement and Concrete Research*, 30(9):1465–1475, 2000.

J. Torrenti, L. Granger, M. Diruy, and P. Genin. Modélisation du retrait du béton en ambiance variable. *Revue française de génie civil*, 1(4):687–698, 1997.

A. Tran, J. Yvonnet, Q.-C. He, C. Toulemonde, and J. Sanahuja. A four-scale homogenization analysis of creep of a nuclear containment structure. *Nuclear Engineering and Design*, 265:712–726, 2013.

H. Tsien. A generalization of Alfrey's theorem for visco-elastic media. *Quarterly of Applied Mathematics*, 8 (1):104–106, 1950.

M. Vandamme and F. Ulm. Nanogranular origin of concrete creep. *Proceedings of the National Academy of Sciences*, 106(26):10552–10557, 2009.

F. Vodák, K. Trtík, V. Sopko, O. Kapičková, and P. Demo. Effect of γ-irradiation on strength of concrete for nuclear-safety structures. *Cement and Concrete Research*, 35(7):1447–1451, 2005.

F. Vodák, V. Vydra, K. Trtík, and O. Kapičková. Effect of gamma irradiation on properties of hardened cement paste. *Materials and Structures*, 44(1):101–107, 2011.

F. Wittmann. Einfluss des feuchtigkeitsgehaltes auf das kriechen des zementsteines. *Rheologica Acta*, 9(2): 282–287, 1970.

T. Wu, İ. Temizer, and P. Wriggers. Multiscale hydro-thermo-chemo-mechanical coupling: Application to alkali–silica reaction. *Computational Materials Science*, 84:381–395, 2014.

O. Zienkiewicz, M. Watson, and I. King. A numerical method of visco-elastic stress analysis. *International Journal of Mechanical Sciences*, 10(10):807–827, 1968.

V. Zubov and A. Ivanov. Expansion of quartz caused by irradiation by fast neutrons. *Soviet Physics Crystallography*, 11:372–374, 1966.